Journal of Micromechanics and Molecular Physics
Vol. 1, Nos. 3 & 4 (2016) 1640011 (27 pages)

DOI: 10.1142/S2424913016400117

World Scientific
www.worldscientific.com

An Eshelbian homogenization solution for a coupled stress-diffusion moving interface problem in composites

Yang Zhang*,†, Xian-Cheng Zhang*,‡, Shan-Tung Tu* and Shaofan Li†,§

*Key Laboratory of Pressure Systems and Safety, Ministry of Education
East China University of Science and Technology
Shanghai, P. R. China

†Department of Civil and Environmental Engineering
University of California at Berkeley, CA, USA
‡xczhang@ecust.edu.cn
§li@ce.berkeley.edu

Received 24 October 2016
Accepted 1 November 2016
Published 29 November 2016

Abstract In this work, we proposed a homogenization model to treat the coupled mechanical-diffusion moving interface problem. The Eshelbian homogenization method is applied to find the effective mechanical properties and diffusivity. On the one hand, the diffusion of solute elements would induce the formation of inclusion phases, affecting the mechanical equilibrium, properties and diffusivity. On the other hand, the stress condition will also have effects on the chemical potential and diffusion process. The coupling of the mechanical and diffusion processes were simulated using the present model, i.e., normal diffusion process and that with previous diffusion treatment. In the former case, thicknesses of outer and inner diffusion parts both increased with time. In the latter case, decomposition of the outer diffusion part might take place to maintain the growth of the inner part.

Keywords Homogenization; micromechanics; diffusion; mechanics; interface.

1. Introduction

It is well known that bilayer structure would be formed during thermal oxidation of titanium, zirconium and their alloys [Dong and Bell, 2000; Güleryüz and Çimenoğlu, 2004; Zumpicchiat *et al.*, 2015; Rosa, 1970; Zhang *et al.*, 2016]. Figure 1 shows the cross-sectional microstructure of Ti-6Al-4V alloy thermally oxidized at 873 K and protected by nickel coating [Zhang *et al.*, 2016]. The original Ti-6Al-4V alloy consisted of epitaxial primary alpha grains and lamellar beta grains. As seen in Fig. 1, the oxidized alloy has been obviously divided into two parts by the interface. Resulted from the absorption of oxygen, some fractions of alpha titanium (α-Ti)

‡,§Corresponding authors.

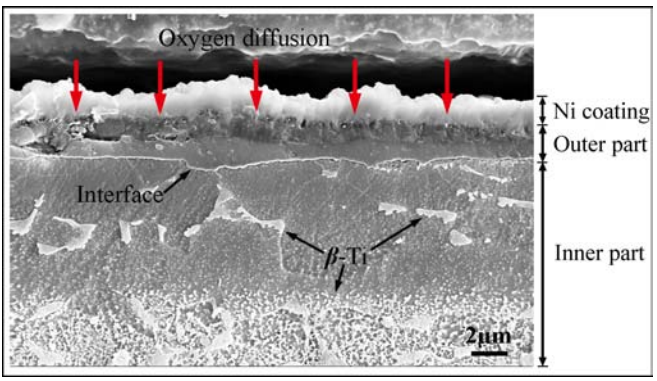

Fig. 1. Cross-sectional microstructure of thermal oxidized Ti-6Al-4V alloy protected by nickel coating [Zhang *et al.*, 2016]. The microstructure is divided into two parts by the interface. The inner part was composed of alpha titanium, beta titanium and the solid solution of alpha titanium and oxygen, i.e., Ti[O], whereas the outer part was the composite of rutile, alumina and Ti[O]. Within the inner part, the white phase was identified as the beta titanium. The alpha titanium and Ti[O] were hard to distinguish from each other by optical method, since their colors are all gray.

and beta titanium (β-Ti) would be transformed to the solid solution of alpha titanium and oxygen, i.e., Ti[O]. Meanwhile, another distinct layer related to oxygen diffusion would be generated beyond the alloy, which was composed of rutile, alumina and Ti[O]. If the phases of α-Ti and Ti[O] were respectively regarded as the matrices of the inner and outer parts, other phases could be identified as inclusions added into the composites. For example, in the inner region, we may regard β-Ti as the inclusion phase, whose diffusion coefficient of oxygen could be expressed as $D_\beta = 330 \times \exp(-58,800/RT)\,\mathrm{cm^2 s^{-1}}$ for the range between 1205 K and 1415 K, in comparison with that of α-Ti as $D_\alpha = 0.778 \cdot \exp(-48,600/RT)\,\mathrm{cm^2 s^{-1}}$ in the same temperature range. R and T are the gas constant and Kelvin temperature. For the outer region, one may regard rutile as the inclusion phase. Of course, still regarding α-Ti and Ti[O] as the matrices for the inner and outer regions, the inclusion phases may also be identified as Ti[O] and alumina, respectively. Generally speaking, this type of problems can be modeled as the diffusion problem with a moving interface between two composites. In fact, there have been long-standing interests in the diffusion problem with a moving interface, owing to its broad applications, such as thermal oxidation, diffusive alloying, transient liquid phase bonding, and some other diffusion-controlled heat or mass transfer processes. In order to solve this problem, differential equations subjected to discontinuity at the interface have been proposed, accompanied with the development of various numerical methods based on phase field method, finite-difference or finite-element methods. Among them, the spatial discretization method by Crank [1957] has shown good accuracy and simplicity, where Lagrange's interpolation formula was employed to evaluate the concentration near moving interface. To achieve even higher accuracy, this method

has been further modified by Lazaridis [1970] and Zhou and North [1993] and Schuh [2000].

Recent research works in the literature [Haftbaradaran *et al.*, 2011; Anand, 2012; Larchè, 1978; Wu, 2001; Villani *et al.*, 2014; Yang, 2005] indicated that the atomic diffusion process was coupled with mechanical stress condition. Modeling approaches on the interaction between diffusion and stress can be mainly divided into two categories. The first category of studies was to investigate the strain and stress generation during the diffusion process. The mechanical stress was proven to be dependent on the concentration of solute elements, since the absorption of interstitial atoms will cause considerable expansion of crystal lattice [Haftbaradaran *et al.*, 2011; Yang, 2005; Bhandakkar and Johnson, 2012]. Meanwhile, the diffusion of solute elements would also lead to phase transformation and induce large strain and stress [Zhang *et al.*, 2014; Maharjan *et al.*, 2012; Zhang *et al.*, 2015]. The second category of studies was to investigate the influence of stress on the diffusion process. For instance, the application of compressive stress will increase the internal energy density and then affect the chemical potential [Anand, 2012; Larchè, 1978; Wu, 2001; Villani *et al.*, 2014], which in turn will affect the diffusivity. Based on the Maxwell-type relationship, one can show that the change of chemical potential is linearly dependent on stress, which is the same as the linear dependence of expansion strain on concentration.

Considering the formation of inclusion phase, the ultimate product of diffusion process is always regarded as inhomogeneous composites of a gradient structure. Consequently, the chemical and mechanical properties were seriously affected by the volume fraction of inclusion phase. From this perspective, the homogenization approach may be employed to predict the effective mechanical properties of the material. In mechanical homogenization theory, the Eshelby's equivalent homogenization principle is widely recognized for its elegance and universality, where the equivalency between an eigenstrain field and an inhomogeneity distribution of a second phase is established, such that the distribution of inhomogeneities could be replaced by the eigenstrain field with the equivalent mechanical effect [Eshelby, 1957]. In particular, for spherical or ellipsoidal inclusions in an infinite elastic medium, the Eshelby tensors have explicit closed-form expressions [Eshelby, 1957; Mura, 1987]. Mori and Tanaka proved that the average strain in the exterior area of a spherical or ellipsoidal inclusion is identically zero [Tanaka and Mori, 1972, 1973]. Based on this theory, the effective mechanical properties may be accurately predicated as the functions of inclusion volume fraction [Weng, 1990]. In recent years, several research works were carried out for the treatment of inhomogeneity problems of coupled problems, e.g., Kuhn *et al.* [2002] and Li and Dunn [1998].

In this work, interaction between diffusion process and mechanical responses of the material is modeled by considering the dependences of diffusivity and elastic tensor on concentration; and we studies the relationship between chemical potential and mechanical stress, and the effect of phase transformation on expansion

strain. The effective diffusivity and mechanical properties are evaluated through the homogenization approach. Based on the Eshelbian homogenization method, we have calculated the variation of concentration, stress and scale thickness by using a modified finite-difference method.

2. Theoretical Framework

2.1. *Description of present model*

Figure 2 schematically shows the diffusion of addition elements into the inhomogeneous material with a moving interface. Resulted from chemical potential gradient, diffusing element will be transferred to the deep inside. Meanwhile, the absorption of diffusing element will promote the transformation from matrix phase (gray) to the inclusion phase (colorful balls). The concentration of elements in each phase is assumed to remain constant. Thus, the dependence of average concentration, c, on volume fraction, f_α, can be expressed as

$$c = \frac{1}{V}\int_V c(\boldsymbol{x})d\boldsymbol{x} = \sum_{\alpha=0}^{n} f_\alpha c_\alpha, \tag{1}$$

where V is the volume of domain, c_α is the concentration in phase α, and $\alpha = 0$ denotes the matrix. Given the inclusion volume fraction or the average concentration, diffusivity and elastic tensors are predicted through homogenization method. The relationship between mechanical behavior and diffusion process is multi-fold. On one side, the absorption of diffusing element will induce severe lattice expansion and affect the mechanical stress distribution. On the other side, due to the chemical potential dependence on mechanical stress, diffusion process is influenced by the stress condition. The material is divided into two major parts by the interface, where the average concentration drops dramatically to produce discontinuity.

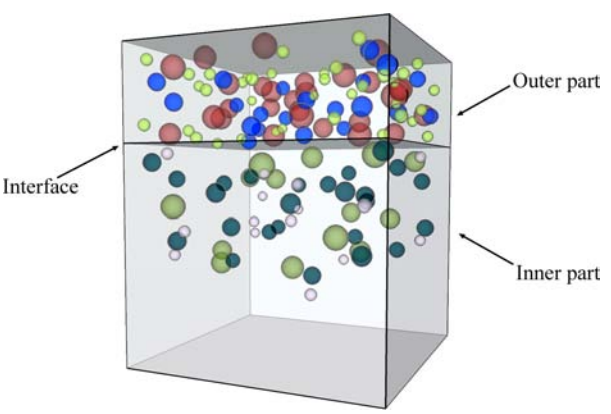

Fig. 2. Illustration of inhomogeneous composites with moving interface. Inclusion phases (colorful balls) are formed due to the absorption of diffusing elements (Color online).

It should be noted that the inclusions formed in the inner and outer parts could be different. The average concentration at the interface remains constant and its location will vary along with time. The interface moving rate is directly determined by the flux difference between the two sides of interface.

2.2. *Effective diffusivity and elastic tensors*

In a steady state case, if there is a diffusion source at point $\boldsymbol{y}$, the divergence of diffusion flux, $\boldsymbol{J}$ at point $\boldsymbol{x}$ can be expressed as

$$J_{i,i}(\boldsymbol{x}) + \delta(\boldsymbol{x} - \boldsymbol{y}) = 0. \tag{2}$$

The Fick's law of diffusion is expressed as

$$J_i(\boldsymbol{x}) = D_{ij} g_j(\boldsymbol{x}) = D_{ij} c_{,j}(\boldsymbol{x}), \tag{3}$$

where $\boldsymbol{g}$ is the concentration gradient and D is the diffusivity tensor. In the isotropic case, the diffusivity tensor may be written as

$$D_{ij} = D\delta_{ij}, \tag{4}$$

where D is the diffusivity and δ_{ij} is the Kronecker delta. If the distribution of concentration is the Green's function $G^{\infty}(\boldsymbol{x} - \boldsymbol{y})$, Eq. (2) is rewritten as

$$D_{ij} G^{\infty}_{,ji}(\boldsymbol{x} - \boldsymbol{y}) + \delta(\boldsymbol{x} - \boldsymbol{y}) = 0. \tag{5}$$

Based on Fourier transformation, the Green's function is obtained as [Li and Wang, 2008],

$$G^{\infty}(\boldsymbol{x} - \boldsymbol{y}) = \frac{1}{4D\pi|\boldsymbol{x} - \boldsymbol{y}|}. \tag{6}$$

Following the definition of eigenstrain, we can define the eigen-gradient for the diffusion process in a composite representative volume element (RVE) as:

$$g^*_i(\boldsymbol{x}) = \begin{cases} g^*_i, & x \in \Omega, \\ 0, & x \in M, \end{cases} \tag{7}$$

which is satisfying

$$J_i(\boldsymbol{x}) = \begin{cases} D^{\alpha}_{ij} g_j(\boldsymbol{x}), & \boldsymbol{x} \in \Omega \\ D^{m}_{ij} g_j(\boldsymbol{x}), & \boldsymbol{x} \in M \end{cases} = \begin{cases} D^{m}_{ij}[g_j(\boldsymbol{x}) - g^*_j(\boldsymbol{x})], & \boldsymbol{x} \in \Omega, \\ D^{m}_{ij} g_j(\boldsymbol{x}), & \boldsymbol{x} \in M. \end{cases} \tag{8}$$

In a quasi-static state, the divergence is identically vanishing, i.e.,

$$J_{i,i}(\boldsymbol{x}) = D_{ij} c_{,ji}(\boldsymbol{x}) - D_{ij} g^*_{j,i}(\boldsymbol{x}) = 0. \tag{9}$$

Thus, the Fourier's inverse transformation of Eq. (9) is

$$\int_{R^3} [D_{ij}\xi_j\xi_i \bar{c}(\boldsymbol{\xi}) + iD_{ij}\xi_i \bar{g}^*_j(\boldsymbol{\xi})] \exp(i\boldsymbol{\xi} \cdot \boldsymbol{x}) d\boldsymbol{\xi} = \boldsymbol{0}. \tag{10}$$

The solution of Eq. (10) in the Fourier space can be expressed as

$$\bar{c}(\boldsymbol{\xi}) = -\frac{iD_{ij}\xi_i \bar{g}^*_j(\boldsymbol{\xi})}{D_{ij}\xi_j\xi_i} = -iD_{ij}\xi_i D^{-1}\xi^{-2}\bar{g}^*_j(\boldsymbol{\xi}). \tag{11}$$

From Eq. (6), the Fourier transformation of the derivative of G^{∞} is

$$\bar{G}^{\infty}_{,i}(\boldsymbol{\xi}) = i\xi_i D^{-1}(2\pi)^{-3}\xi^{-2} = i\xi_i \bar{G}^{\infty}(\boldsymbol{\xi}). \tag{12}$$

Then the inverse transformation of Eq. (11) can be obtained by the inverse Fourier transform,

$$\begin{aligned} c(\boldsymbol{x}) &= -(2\pi)^3 \int_{R^3} D_{ij}\bar{G}^{\infty}_{,i}(\boldsymbol{\xi})\bar{g}^{*}_{j}(\boldsymbol{\xi}) \exp(i\boldsymbol{\xi}\cdot\boldsymbol{x}) d\boldsymbol{\xi} \\ &= -\int_{R^3} D_{ij} g^{*}_{j}(\boldsymbol{y}) G^{\infty}_{,i}(\boldsymbol{x}-\boldsymbol{y}) d\boldsymbol{y}. \end{aligned} \tag{13}$$

Assuming that $\boldsymbol{g}^{*}$ is constant, the Eshelby tensor can then be obtained as

$$S_{mj}(\boldsymbol{x}) = \int_{\Omega} -D_{ij} G^{\infty}_{,im}(\boldsymbol{x}-\boldsymbol{y}) d\boldsymbol{y} = \begin{cases} S^{I}_{mj}, & \boldsymbol{x}\in\Omega, \\ S^{E}_{mj}, & \boldsymbol{x}\in M, \end{cases} \tag{14}$$

which provides the solution for the induced gradient of the concentration field,

$$g_m(\boldsymbol{x}) = c_{,m}(\boldsymbol{x}) = S_{mj} g^{*}_{j}. \tag{15}$$

Denoting

$$\phi(\boldsymbol{x}-\boldsymbol{y}) = \int_{\Omega} \frac{1}{|\boldsymbol{x}-\boldsymbol{y}|} \mathrm{d}\Omega_y, \tag{16}$$

we can express the Eshelby tensor for diffusion as

$$\begin{aligned} S_{mj} &= -\frac{1}{4\pi} \int_{\Omega} \frac{\partial^2}{\partial x_m \partial x_j} \frac{1}{|\boldsymbol{x}-\boldsymbol{y}|} \mathrm{d}\Omega_y \\ &= -\frac{1}{4\pi} \frac{\partial^2}{\partial x_m \partial x_j} \int_{\Omega} \frac{1}{|\boldsymbol{x}-\boldsymbol{y}|} \mathrm{d}\Omega_y = -\frac{1}{4\pi}\phi_{,mj}. \end{aligned} \tag{17}$$

Actually, for a spherical inclusion, one may find the potential function in explicit form

$$\phi(\boldsymbol{x}) = \begin{cases} -\dfrac{2\pi}{3}(|\boldsymbol{x}|^2 - 3a^2), & \boldsymbol{x}\in\Omega, \\ \dfrac{4\pi a^3}{3|\boldsymbol{x}|}, & \boldsymbol{x}\in M. \end{cases} \tag{18}$$

Then Eshelby tensor can then be written as

$$S_{mj} = \begin{cases} \dfrac{1}{3}\delta_{ij}, & \boldsymbol{x}\in\Omega, \\ \dfrac{a^3}{3|\boldsymbol{x}|^3}\delta_{mj} - \dfrac{a^3}{|\boldsymbol{x}|^5} x_m x_j, & \boldsymbol{x}\in M. \end{cases} \tag{19}$$

For the exterior area, Eshelby tensor is a function of location $\boldsymbol{x}$. However, from Eq. (19), one may find that the integral of S_{mj} in the exterior is

$$\int_{M} S^{E}_{mj}(\boldsymbol{x}) d\boldsymbol{x} = 0. \tag{20}$$

Thus, the average value of $\boldsymbol{g}$ in any exterior area of the inclusion can be proven to be zero.

$$\int_M g_m(\boldsymbol{x})d\boldsymbol{x} = g_m^* \int_M^{S_{mj}^E(\boldsymbol{x})} d\boldsymbol{x} = 0. \tag{21}$$

Actually, the same observation has been made for mechanical properties in a composite material according to Tanaka–Mori lemma [Tanaka and Mori, 1972]. If there are three spheres satisfying $\Omega_1 \subset \Omega_2 \subset \Omega_3$, the integration of gradient in the region $\Omega_3 - \Omega_2$ is

$$\begin{aligned}\int_{\Omega_3-\Omega_2} g_m(\boldsymbol{x})d\boldsymbol{x} &= \int_{\Omega_3-\Omega_2} g_m^* S_{mj}^E(\boldsymbol{x})d\boldsymbol{x} \\ &= \int_{\Omega_3-\Omega_2} g_m^* \int_{\Omega_1} -D_{ij}G_{,im}^{\infty}(\boldsymbol{x}-\boldsymbol{y})d\boldsymbol{y}d\boldsymbol{x}. \end{aligned}\tag{22}$$

Changing the order of integration in Eq. (22), it is obtained as

$$\begin{aligned}\int_{\Omega_3-\Omega_2} g_m(\boldsymbol{x})d\boldsymbol{x} &= \int_{\Omega_1} g_m^* \int_{\Omega_3} -D_{ij}G_{,im}^{\infty}(\boldsymbol{x}-\boldsymbol{y})d\boldsymbol{x}d\boldsymbol{y} \\ &\quad - \int_{\Omega_1} g_m^* \int_{\Omega_2} -D_{ij}G_{,im}^{\infty}(\boldsymbol{x}-\boldsymbol{y})d\boldsymbol{x}d\boldsymbol{y} \\ &= \int_{\Omega_1} [g_m^* S_{mj}^I(\Omega_3) - g_m^* S_{mj}^I(\Omega_2)]d\boldsymbol{y}. \end{aligned}\tag{23}$$

Since the Eshelby tensor only depends on the material properties, we found that the average gradient in any exterior area of the inclusion vanishes,

$$\int_{\Omega_2-\Omega_1} g_i(\boldsymbol{x})d\boldsymbol{x} = \int_{\Omega_3-\Omega_2} g_i(\boldsymbol{x})d\boldsymbol{x} = 0. \tag{24}$$

When the matrix is the dominated phase, we donate the mean gradient in matrix phase as the mean field of the entire volume

$$\langle \boldsymbol{g} \rangle_M \approx \langle \boldsymbol{g} \rangle_V. \tag{25}$$

Then average gradient in the inclusion is

$$\langle \boldsymbol{g} \rangle_\Omega = \langle \boldsymbol{g} \rangle_M + \boldsymbol{S}^I \cdot \boldsymbol{g}^*. \tag{26}$$

According to the Elshelby's homogenization theory,

$$\langle \boldsymbol{J} \rangle_\Omega = \boldsymbol{D}^\alpha \cdot \langle \boldsymbol{g} \rangle_\Omega = \boldsymbol{D}^\alpha \cdot (\langle \boldsymbol{g} \rangle_\Omega - \langle \boldsymbol{g}^* \rangle). \tag{27}$$

Then the relationship between $\langle \boldsymbol{g} \rangle_\Omega$ and $\langle \boldsymbol{g} \rangle_V$ is

$$\langle \boldsymbol{g} \rangle_\Omega = (\boldsymbol{D}^m - \boldsymbol{D}^\alpha)^{-1} \cdot \boldsymbol{D}^m \cdot [(\boldsymbol{D}^m - \boldsymbol{D}^\alpha)^{-1} \cdot \boldsymbol{D}^m - \boldsymbol{S}^I]^{-1} \cdot \langle \boldsymbol{g} \rangle_V. \tag{28}$$

The average gradient and diffusion flux are respectively

$$\langle \boldsymbol{J} \rangle_V = (1-f_\alpha)\langle \boldsymbol{J} \rangle_M + f\langle \boldsymbol{J} \rangle_\Omega = (1-f_\alpha)\boldsymbol{D}^m \cdot \langle \boldsymbol{g} \rangle_m + f\boldsymbol{D}^\Omega \cdot \langle \boldsymbol{g} \rangle_\Omega, \tag{29}$$

$$\langle \boldsymbol{g} \rangle_V = (1-f_\alpha)\langle \boldsymbol{g} \rangle_M + f_\alpha \langle \boldsymbol{g} \rangle_\Omega. \tag{30}$$

Considering that

$$\langle \boldsymbol{J} \rangle_V = \bar{\boldsymbol{D}} \cdot \langle \boldsymbol{g} \rangle_V. \tag{31}$$

Thus, the effective diffusivity tensor is

$$\begin{aligned}\bar{\boldsymbol{D}} = &\{(1-f_\alpha)\boldsymbol{D}^m - f_\alpha \boldsymbol{D}^\alpha \cdot (\boldsymbol{D}^m - \boldsymbol{D}^\alpha)^{-1} \cdot \boldsymbol{D}^m \cdot [(\boldsymbol{D}^m - \boldsymbol{D}^\alpha)^{-1} \cdot \boldsymbol{D}^m - \boldsymbol{S}^I]^{-1}\} \\ &\times \{(1-f_\alpha)\boldsymbol{I}^{(2)} - f_\alpha (\boldsymbol{D}^m - \boldsymbol{D}^\alpha)^{-1} \cdot \boldsymbol{D}^m \cdot [(\boldsymbol{D}^m - \boldsymbol{D}^\alpha)^{-1} \cdot \boldsymbol{D}^m - \boldsymbol{S}^I]^{-1}\}^{-1}.\end{aligned} \tag{32}$$

In general, for composite with n inclusion phases, Eq. (27) changes to

$$\begin{aligned}\bar{\boldsymbol{D}} = &\left\{ \left(1 - \sum_{\alpha=1}^{n} f_\alpha\right) \boldsymbol{D}^m - \sum_{\alpha=1}^{n} f_\alpha \boldsymbol{D}^\alpha \cdot (\boldsymbol{D}^m - \boldsymbol{D}^\alpha)^{-1} \right. \\ &\left. \cdot \boldsymbol{D}^m \cdot [(\boldsymbol{D}^m - \boldsymbol{D}^\alpha)^{-1} \cdot \boldsymbol{D}^m - \boldsymbol{S}^I]^{-1} \right\} \\ &\times \left\{ \left(1 - \sum_{\alpha=1}^{n} f_\alpha\right) \boldsymbol{I}^{(2)} - \sum_{\alpha=1}^{n} f_\alpha (\boldsymbol{D}^m - \boldsymbol{D}^\alpha)^{-1} \right. \\ &\left. \cdot \boldsymbol{D}^m \cdot [(\boldsymbol{D}^m - \boldsymbol{D}^\alpha)^{-1} \cdot \boldsymbol{D}^m - \boldsymbol{S}^I]^{-1} \right\}^{-1}.\end{aligned} \tag{33}$$

If there is a concentrated mechanical load at point $\boldsymbol{y}$, direction of which is mth direction, the divergence of stress can be expressed as

$$\sigma_{ij,j}(\boldsymbol{x}) + \delta(\boldsymbol{x} - \boldsymbol{y})\delta_{mi} = 0. \tag{34}$$

The linear relationship among concentration, gradient and flux is

$$\sigma_{ij} = C_{ijmn}\varepsilon_{mn} = \frac{1}{2} C_{ijmn}(u_{i,j} + u_{j,i}). \tag{35}$$

If the distribution of deformation is the Green's function $G^\infty_{mi}(\boldsymbol{x} - \boldsymbol{y})$, Eq. (36) is obtained

$$C_{ijkl} G^\infty_{mk,lj}(\boldsymbol{x} - \boldsymbol{y}) + \delta(\boldsymbol{x} - \boldsymbol{y})\delta_{mi} = 0. \tag{36}$$

For the isotropic case, the Green's function is

$$G^\infty_{ij}(\boldsymbol{x} - \boldsymbol{y}) = \frac{(\lambda + \mu)}{8\pi\mu z(\lambda + 2\mu)} \left[\frac{\lambda + 3\mu}{\lambda + \mu} \delta_{ij} + \frac{(x_i - y_i)(x_j - y_j)}{|\boldsymbol{x} - \boldsymbol{y}|^2} \right], \tag{37}$$

where λ and μ are Lame constants. The equilibrium equation is an equivalent form of zero divergence of Cauchy stress tensor, i.e.,

$$\sigma_{ij,j} = 0. \tag{38}$$

The elastic relationship between stress and strain is

$$\sigma_{ij} = C_{ijkl}\varepsilon^e_{kl} = C_{ijkl} u_{k,l}. \tag{39}$$

Define the eigen strain as

$$\varepsilon_{kl}^{*}(\boldsymbol{x}) = \begin{cases} \varepsilon_{kl}^{*}, & \boldsymbol{x} \in \Omega, \\ 0, & \boldsymbol{x} \in M, \end{cases} \tag{40}$$

satisfying

$$\sigma_i(\boldsymbol{x}) = \begin{cases} C_{ijkl}^{\alpha}\varepsilon_{kl}^{e}(\boldsymbol{x}), & \boldsymbol{x} \in \Omega \\ C_{ijkl}^{m}\varepsilon_{kl}^{e}(\boldsymbol{x}), & \boldsymbol{x} \in M \end{cases} = \begin{cases} C_{ijkl}^{\alpha}[\varepsilon_{kl}(\boldsymbol{x}) - \varepsilon_{kl}^{*}(\boldsymbol{x})], & \boldsymbol{x} \in \Omega, \\ C_{ijkl}^{\alpha}\varepsilon_{kl}(\boldsymbol{x}), & \boldsymbol{x} \in M. \end{cases} \tag{41}$$

Within the inclusion, if $\boldsymbol{\varepsilon}^{*}$ is independent of $\boldsymbol{x}$, the Eshelby tensor can be determined as

$$S_{ikmn} = -\int_{\Omega} C_{jlmn} G_{ij,lk}^{\infty}(\boldsymbol{x} - \boldsymbol{y}) d\boldsymbol{y} = \begin{cases} S_{ikmn}^{I}, & \boldsymbol{x} \in \Omega, \\ S_{ikmn}^{E}, & \boldsymbol{x} \in M, \end{cases} \tag{42}$$

satisfying

$$\varepsilon_{ik} = u_{i,k} = S_{ikmn}\varepsilon_{mn}^{*}. \tag{43}$$

For the interior area of inclusion, Eshelby tensor is given by [Li and Wang, 2008]

$$S_{ijkl}^{I} = \frac{5v_0 - 1}{15(1 - v_0)}\delta_{ij}\delta_{kl} + \frac{4 - 5v_0}{15(1 - v_0)}(\delta_{ik}\delta_{jl} + \delta_{jk}\delta_{il}), \tag{44}$$

$$\begin{aligned} S_{ijkl}^{E} = {} & \frac{a^3}{30(1 - v_0)|\boldsymbol{x}|^3}\left(\frac{3a^2}{|\boldsymbol{x}|^2} + 10v_0 - 5\right)\delta_{ij}\delta_{jk} \\ & + \left(\frac{3a^2}{|\boldsymbol{x}|^2} - 10v_0 + 5\right)(\delta_{ik}\delta_{jl} + \delta_{il}\delta_{jk}) + \frac{15(|\boldsymbol{x}|^2 - a^2)}{|\boldsymbol{x}|^4}\delta_{ij}x_k x_l \\ & + \frac{15(|\boldsymbol{x}|^2 - 2v_0|\boldsymbol{x}|^2 - a^2)}{|\boldsymbol{x}|^4}\delta_{kl}x_i x_j + \frac{15(v_0|\boldsymbol{x}|^2 - a^2)}{|\boldsymbol{x}|^4} \\ & \times (\delta_{ik}x_j x_l + \delta_{il}x_j x_k + \delta_{jk}x_i x_l + \delta_{jl}x_i x_k) \\ & + \frac{15(-5v_0|\boldsymbol{x}|^2 + 7a^2)}{|\boldsymbol{x}|^4}x_i x_j x_k x_l. \end{aligned} \tag{45}$$

The Mori–Tanaka model on effective mechanical properties can be applied directly here, i.e.,

$$\bar{\boldsymbol{C}} = \sum_{\alpha=0}^{n}[f_\alpha \boldsymbol{C}_\alpha : \boldsymbol{A}_\alpha : (\boldsymbol{A}_\alpha - \boldsymbol{S}^I)^{-1}] : \left[\sum_{\alpha=0}^{n}(f_\alpha \boldsymbol{A}_\alpha)\right]^{-1}, \tag{46a}$$

$$\boldsymbol{A}_\alpha = (\boldsymbol{C}_0 - \boldsymbol{C}_\alpha)^{-1} : \boldsymbol{C}_0 = \frac{K_0}{K_0 - K_\alpha}\boldsymbol{E}^{(1)} + \frac{G_0}{G_0 - G_\alpha}\boldsymbol{E}^{(2)}, \tag{46b}$$

$$\boldsymbol{E}^{(1)} = \frac{1}{3}\boldsymbol{I}^{(2)} \otimes \boldsymbol{I}^{(2)}, \tag{46c}$$

$$\boldsymbol{E}^{(2)} = -\frac{1}{3}\boldsymbol{I}^{(2)} \otimes \boldsymbol{I}^{(2)} + \boldsymbol{I}^{(4s)}, \tag{46d}$$

where $\boldsymbol{I}^{(2)}$ and $\boldsymbol{I}^{(4s)}$ are respectively the second-order unit tensor and fourth-order symmetric tensor. Subsequently, the effective volume elastic modulus and shear modulus are respectively

$$\bar{K} = \frac{\sum_{\alpha=0}^{n}\left[\frac{f_\alpha K_\alpha}{(1+v_0)K_\alpha+2(1-2v_0)K_0}\right]}{\sum_{\alpha=0}^{n}\left[\frac{f_\alpha}{(1+v_0)K_\alpha+2(1-2v_0)K_0}\right]}, \tag{47}$$

$$\bar{G} = \frac{\sum_{\alpha=0}^{n}\left[\frac{f_\alpha G_\alpha}{2(4-5v_0)G_\alpha+(7-5v_0)G_0}\right]}{\sum_{\alpha=0}^{n}\left[\frac{f_\alpha}{2(4-5v_0)G_\alpha+(7-5v_0)K_0}\right]}. \tag{48}$$

Accordingly, the effective Young's modulus, $\bar{E}$, and Poisson's ratio, $\bar{v}$, can be obtained according to the following equations,

$$\bar{E} = \frac{9\bar{K}\bar{G}}{3\bar{K}+\bar{G}}, \tag{49}$$

$$\bar{v} = \frac{3\bar{K}-2\bar{G}}{2(3\bar{K}+\bar{G})}. \tag{50}$$

2.3. *Expansion strain in micro and macroscales*

The solution of oxygen atoms induces the phase transformation and lattice expansion within the inclusion domain, which is expressed as

$$\Delta\boldsymbol{\varepsilon}^{\alpha}(\boldsymbol{x}) = \begin{cases} \Delta\boldsymbol{\varepsilon}^{\alpha}, & \boldsymbol{x}\in\Omega, \\ 0, & \boldsymbol{x}\in M. \end{cases} \tag{51}$$

However, due to the compression from the matrix, the actual expansion strain related to solution, $\boldsymbol{\varepsilon}^{c}$, is smaller than $\Delta\boldsymbol{\varepsilon}$. Considering the expansion induced by solution, $\boldsymbol{\varepsilon}^{*}$ is replaced with the superposition of $\Delta\boldsymbol{\varepsilon}^{\alpha}$ and $\boldsymbol{\varepsilon}^{*}$. Consequently, the disturbance stress within the inclusion domain can be expressed as

$$\boldsymbol{\sigma}^{d}(\boldsymbol{x}) = \boldsymbol{C}^{M} : [\boldsymbol{\varepsilon}^{d}(\boldsymbol{x}) - \boldsymbol{\varepsilon}^{*} - \Delta\boldsymbol{\varepsilon}^{\alpha}] = \boldsymbol{C}^{\alpha} : [\boldsymbol{\varepsilon}^{d}(\boldsymbol{x}) - \Delta\boldsymbol{\varepsilon}^{\alpha}], \quad \boldsymbol{x}\in\Omega. \tag{52}$$

And the disturbance strain within the inclusion domain is given by

$$\boldsymbol{\varepsilon}^{d} = \boldsymbol{S}^{I} : (\boldsymbol{\varepsilon}^{*} + \Delta\boldsymbol{\varepsilon}^{\alpha}), \quad \boldsymbol{x}\in\Omega. \tag{53}$$

Combining the above two equations, it can be obtained as

$$\boldsymbol{\varepsilon}^{d}(\boldsymbol{x}) = \boldsymbol{S}^{I} : [\boldsymbol{C}^{M} : (\boldsymbol{I}^{(4s)} - \boldsymbol{S}^{I}) + \boldsymbol{C}^{\alpha} : \boldsymbol{S}^{I}]^{-1} : \boldsymbol{C}^{\alpha} : \Delta\boldsymbol{\varepsilon}^{\alpha}, \quad \boldsymbol{x}\in\Omega. \tag{54}$$

For simplicity, Eq. (44) is rewritten as

$$\boldsymbol{S}^{I} = \frac{1+v_0}{3(1-v_0)}\boldsymbol{E}^{(1)} + \frac{2(4-5v_0)}{15(1-v_0)}\boldsymbol{E}^{(2)}. \tag{55}$$

In the macroscale, the expansion strain related to solution is expressed as

$$\boldsymbol{\varepsilon}^{c} = (c-c_{\mathrm{ref}})\frac{d\boldsymbol{\varepsilon}^{c}}{dc} + \boldsymbol{\varepsilon}^{c}_{\mathrm{ref}} = (c-c_{\mathrm{ref}})\boldsymbol{H} + \boldsymbol{\varepsilon}^{c}_{\mathrm{ref}}, \tag{56}$$

where $\boldsymbol{\varepsilon}^c_{\text{ref}}$ is the reference strain corresponding to reference concentration, c_{ref}. In a particular isotropic case, $\boldsymbol{H}$ is generally written as

$$\boldsymbol{H} = H\boldsymbol{I}^{(2)}. \tag{57}$$

The average strain is

$$\langle\boldsymbol{\varepsilon}\rangle_V = \frac{1}{V}\int_V \boldsymbol{\varepsilon}(\boldsymbol{x})dV = \sum_{\alpha=0}^{n}\frac{V_\alpha}{V}\left(\frac{1}{V_\alpha}\int_{V_\alpha}\boldsymbol{\varepsilon}(\boldsymbol{x})dV\right) = \sum_{\alpha=0}^{n} f_\alpha\langle\boldsymbol{\varepsilon}\rangle_\alpha + \boldsymbol{\varepsilon}^c_{\text{ref}}. \tag{58}$$

Increasing the average concentration from c_{ref} to c, the expansion strain can be predicted as

$$\boldsymbol{\varepsilon}^c - \boldsymbol{\varepsilon}^c_{\text{ref}} = \langle\boldsymbol{\varepsilon}\rangle = \sum_{\alpha=0}^{n}(f_\alpha\langle\boldsymbol{\varepsilon}\rangle_\alpha) = \sum_{\alpha=1}^{n}(f_\alpha\langle\boldsymbol{\varepsilon}^d\rangle_\alpha) = \sum_{\alpha=1}^{n}(f_\alpha\langle\boldsymbol{\varepsilon}^d\rangle_\alpha) + f_0\langle\boldsymbol{\varepsilon}^d\rangle_0. \tag{59}$$

As mentioned above, the average disturbance strain in the exterior area of an inclusion is zero. If the composite is composed of matrix and unique inclusion phase, the average strain due to phase transformation is

$$\begin{aligned}\boldsymbol{\varepsilon}^c - \boldsymbol{\varepsilon}^c_{\text{ref}} = f_\alpha\Bigg[&\frac{3K_\alpha}{3K_\alpha + 4G_0}\boldsymbol{E}^{(1)} \\ &+ \frac{6G_\alpha(K_0 + 2G_0)}{G_0(9K_0 + 8G_0) + 6G_\alpha(K_0 + 2G_0)}\boldsymbol{E}^{(2)}\Bigg] : \Delta\boldsymbol{\varepsilon}^\alpha.\end{aligned} \tag{60}$$

In an isotropic case, $\Delta\boldsymbol{\varepsilon}^\alpha$ is simplified to

$$\Delta\boldsymbol{\varepsilon}^\alpha = \Delta\varepsilon^\alpha\boldsymbol{I}. \tag{61}$$

It is found that the product of $\boldsymbol{E}$-base and $\Delta\boldsymbol{\varepsilon}^\alpha$ is

$$\begin{aligned}\boldsymbol{E}^{(1)} : \Delta\boldsymbol{\varepsilon}^\alpha &= \left(\frac{1}{3}\delta_{ij}\delta_{kl}\boldsymbol{e_i}\otimes\boldsymbol{e_j}\otimes\boldsymbol{e_k}\otimes\boldsymbol{e_l}\right) : (\delta_{mn}\Delta\varepsilon^\alpha\boldsymbol{e}_m\otimes\boldsymbol{e}_n) \\ &= \delta_{ij}\Delta\varepsilon^\alpha\boldsymbol{e_i}\otimes\boldsymbol{e_j},\end{aligned} \tag{62}$$

$$\begin{aligned}\boldsymbol{E}^{(2)} : \Delta\boldsymbol{\varepsilon}^\alpha = &\left[\left(-\frac{1}{3}\delta_{ij}\delta_{kl} + \frac{1}{2}\delta_{ik}\delta_{jl} + \frac{1}{2}\delta_{il}\delta_{jl}\right)\boldsymbol{e_i}\otimes\boldsymbol{e_j}\otimes\boldsymbol{e_k}\otimes\boldsymbol{e_l}\right] \\ &: (\delta_{mn}\Delta\varepsilon^\alpha\boldsymbol{e}_m\otimes\boldsymbol{e}_n) = 0.\end{aligned} \tag{63}$$

Thus, the disturbance strain can be rewritten as

$$\varepsilon^c_{ij} - (\varepsilon^c_{\text{ref}})_{ij} = \frac{3f_\alpha K_\alpha}{3K_\alpha + 4G_0}\delta_{ij}\Delta\varepsilon^\alpha = \frac{3(c - c_M)K_\alpha}{(c_\alpha - c_M)(3K_\alpha + 4G_0)}\delta_{ij}\Delta\varepsilon^\alpha. \tag{64}$$

Then the expansion strain in the macroscale is proportional to the lattice expansion strain in the microscale. And then $\boldsymbol{H}$ is obtained as

$$\boldsymbol{H} = \frac{\partial(\boldsymbol{\varepsilon}^c - \boldsymbol{\varepsilon}^c_{\text{ref}})}{\partial c} = \frac{3K_\alpha\Delta\boldsymbol{\varepsilon}^\alpha}{(c_\alpha - c_M)(3K_\alpha + 4G_0)}\boldsymbol{I}^{(2)}. \tag{65}$$

2.4. *Stress in micro and macroscales*

In a macroscale, the mechanical boundary condition is given by

$$\boldsymbol{\sigma}(\boldsymbol{x}) = \boldsymbol{\sigma}^t \cdot \boldsymbol{n}, \quad \boldsymbol{x} \in \partial V, \tag{66}$$

where ∂V is boundary, $\boldsymbol{n}$ is the normal vector, $\boldsymbol{\sigma}^t$ is the stress in macroscale. And the elastic strain related to $\boldsymbol{\sigma}^t$ is,

$$\boldsymbol{\varepsilon}^t = \bar{M} : \boldsymbol{\sigma}^t, \tag{67}$$

where $\bar{M}$ is the effective compliance tensor. In a plane-stress state, the stress equilibrium can be expressed as

$$\int_{\partial V_m} \boldsymbol{\sigma}^t dS = A \int_h \boldsymbol{\sigma}^t dx_3 = 0, \tag{68}$$

where A is the perimeter plane normal to x_3, h is the material thickness. In a macroscale, the total strain is regarded as the superposition of $\boldsymbol{\varepsilon}^t$ and $\boldsymbol{\varepsilon}^c$. Then the macro-stress can be expressed as

$$\boldsymbol{\sigma}^t(x_3) = \bar{M}^{-1} : \boldsymbol{\sigma}^t = \bar{C}(x_3) : \boldsymbol{\varepsilon}^t(x_3) = \bar{C}(x_3) : [\boldsymbol{\varepsilon}(x_3) - (c - c_{\text{ref}})\boldsymbol{H} - \boldsymbol{\varepsilon}_{\text{ref}}(x_3)] \tag{69}$$

In a biaxial plane-stress state, the components of stress satisfies

$$\sigma^t_{11} = \sigma^t_{22}, \tag{70}$$

$$\sigma^t_{33} = \sigma^t_{12} = \sigma^t_{13} = \sigma^t_{23} = 0. \tag{71}$$

Combining Eqs. (67)–(71), the normal strain in x_1 and x_2 directions are

$$\varepsilon_{11} = \varepsilon_{22} = \frac{\int_h \frac{\bar{E}(x_3)}{1-\bar{v}(x_3)}[(c - c_{\text{ref}})H + \varepsilon_{\text{ref}}]dx_3}{\int_h \frac{\bar{E}(x_3)}{1-\bar{v}(x_3)}dx_3}. \tag{72}$$

The normal strain in x_3 direction is

$$\varepsilon_{33}(z) = \frac{2[1 + \bar{v}(x_3)]}{1 - \bar{v}(x_3)}[(c - c_{\text{ref}})H + \varepsilon_{\text{ref}}] - \frac{2\bar{v}(x_3)}{1 - \bar{v}(x_3)}\varepsilon_{11}. \tag{73}$$

The normal stresses in x_1 and x_2 directions are

$$\sigma^t_{11}(x_3) = \sigma^t_{22}(x_3) = \frac{\bar{E}(x_3)}{1 - \bar{v}(x_3)}[\varepsilon_{11}(x_3) - (c - c_{\text{ref}})H - \varepsilon^c_{\text{ref}}]. \tag{74}$$

Then the total stress at location $\boldsymbol{x}$ is the superposition of $\boldsymbol{\sigma}^t$ and $\boldsymbol{\sigma}^d$

$$\boldsymbol{\sigma}(\boldsymbol{x}) = \langle \boldsymbol{\sigma} \rangle + \boldsymbol{\sigma}^d(\boldsymbol{x}). \tag{75}$$

Based on Gaussian divergence theorem, $\langle \boldsymbol{\sigma} \rangle$ is proven to be equal to $\boldsymbol{\sigma}^t$. Subsequently, $\boldsymbol{\sigma}^d$ can be obtained according to the Eshelby's homogenization theory.

2.5. *Coupled mechanical-diffusion problem*

In a stress-free state, the free energy, ψ, can be expressed in the following standard form,

$$\psi(c) = \frac{E_f c}{\eta} + \frac{RT}{\eta}[c\ln c + (1-c)\ln(1-c)], \tag{76}$$

where E_f is the formation enthalpy, c is the dimensionless concentration, η is the molar volume of the matrix lattice. For dilute solution, μ_0 is the derivative of ψ with respect to c, i.e.,

$$\mu_0(c) = \frac{\partial \psi}{\partial c} = \frac{RT}{\eta}\left[\ln\left(\frac{c}{1-c}\right) + \frac{E_f}{RT}\right]. \tag{77}$$

The linear variation of μ along with $\boldsymbol{\sigma}^t$ is

$$\mu = \mu_0 - \boldsymbol{\sigma}^t : \boldsymbol{H}, \tag{78}$$

where μ_0 is the reference chemical potential independent of stress. Thus, the equilibrium concentration is dependent on stress state, i.e.,

$$\frac{c_{\text{eq}}}{1-c_{\text{eq}}} = \exp\left(\frac{\mu_0\eta}{RT} - \frac{E_f}{RT}\right)\exp\left(\frac{\eta}{RT}\boldsymbol{H} : \boldsymbol{\sigma}^t\right). \tag{79}$$

Defining $c = \exp(\frac{\mu_0\eta}{RT} - \frac{E_f}{RT})$, when $\exp(\frac{\eta}{RT}\boldsymbol{H} : \boldsymbol{\sigma}^t)$ approaches to 1,

$$c_{\text{eq}} \approx c + \frac{c\eta}{RT}\boldsymbol{H} : \boldsymbol{\sigma}^t. \tag{80}$$

Then the total strain is expressed as

$$\boldsymbol{\varepsilon} = \boldsymbol{\varepsilon}^t + \boldsymbol{\varepsilon}^c = \bar{\boldsymbol{M}} : \boldsymbol{\sigma}^t + (c_{\text{eq}} - c)\boldsymbol{H} + (c - c_{\text{ref}})\boldsymbol{H} + \boldsymbol{\varepsilon}^c_{\text{ref}}, \tag{81}$$

or

$$\boldsymbol{\varepsilon} = \left[\bar{\boldsymbol{M}} + \frac{c\eta}{RT}\boldsymbol{H}\otimes\boldsymbol{H}\right] : \boldsymbol{\sigma}^t + (c - c_{\text{ref}})\boldsymbol{H} + \boldsymbol{\varepsilon}^c_{\text{ref}}. \tag{82}$$

Thus, $\bar{\boldsymbol{M}}$ is modified to $\bar{\bar{\boldsymbol{M}}}$ if the effect of stress on equilibrium concentration is considered,

$$\bar{\bar{\boldsymbol{M}}}_{ijkl}(c) = \left\{-\frac{\bar{v}}{\bar{E}} + \frac{c\eta}{RT}\left[\frac{3K_\alpha\Delta\varepsilon^\alpha}{(c_\alpha - c_M)(3K_\alpha + 4G_0)}\right]^2\right\}\delta_{ij}\delta_{kl} + \frac{1}{2\bar{G}}(\delta_{ik}\delta_{jl} + \delta_{il}\delta_{jk}). \tag{83}$$

From Eq. (83), the following equations are obtained:

$$\bar{\bar{E}}(c) = \bar{E}\left\{1 + \frac{\bar{E}\eta c}{RT}\left[\frac{3K_\alpha\Delta\varepsilon^\alpha}{(c_\alpha - c_M)(3K_\alpha + 4G_0)}\right]^2\right\}^{-1}, \tag{84}$$

$$\bar{\bar{v}}(c) = \left\{\bar{v} - \frac{\bar{E}\eta c}{RT}\left[\frac{3K_\alpha\Delta\varepsilon^\alpha}{(c_\alpha - c_M)(3K_\alpha + 4G_0)}\right]^2\right\}$$

$$\times \left\{ 1 + \frac{\bar{E}\eta c}{RT} \left[\frac{3K_\alpha \Delta\varepsilon^\alpha}{(c_\alpha - c_M)(3K_\alpha + 4G_0)} \right]^2 \right\}^{-1}, \tag{85}$$

$$\bar{\bar{G}}(c) = \bar{G}. \tag{86}$$

In a general approach, the diffusion flux can be expressed as

$$\boldsymbol{J} = \frac{\partial \varphi}{\partial \nabla \mu_{ox}}, \tag{87}$$

$$\varphi = \frac{\bar{D}\eta c(1-c)}{2RT} \boldsymbol{I}^{(2)} : (\nabla\mu \otimes \nabla\mu). \tag{88}$$

In the isotropic case, the flux is written as

$$\boldsymbol{J} = -\bar{D}\nabla c + \frac{3\bar{D}K_\alpha \Delta\varepsilon^\alpha}{RT(c_\alpha - c_0)(3K_\alpha + 4G_0)} c(1-c)\nabla tr(\boldsymbol{\sigma}^t). \tag{89}$$

Equation (89) is regarded as the modification of Fick's second law. And the variation of concentration with respect to time is

$$\frac{\partial c}{\partial t} = -\nabla \cdot \boldsymbol{J}. \tag{90}$$

Substituting Eq. (89) into (90), Eq. (90) can be rewritten in an explicit form,

$$\frac{\partial c}{\partial t} = \nabla\bar{D} \cdot \nabla c + \bar{D}\nabla^2 c - \frac{H\eta}{RT} c(1-c)\nabla\bar{D} \cdot \nabla \mathrm{tr}(\boldsymbol{\sigma}^t) - \frac{\bar{D}\eta H}{RT}(1-2c)\nabla c \cdot \nabla \mathrm{tr}(\boldsymbol{\sigma}^t)$$
$$- \frac{H\eta}{RT}\bar{D}c(1-c)\nabla^2 \mathrm{tr}(\boldsymbol{\sigma}^t). \tag{91}$$

2.6. *Initial and boundary conditions*

Denoting L_1 as the interface and L_2 as the right boundary, the boundary conditions are given by

$$\begin{cases} c(0,t) = c_{s1}, \\ c(L_1,t) = c_{\mathrm{ref1}}, \\ c(L_1,t) = c_{s2}, \\ \left.\dfrac{dc}{dx_3}\right|_{x_3=L_2} = 0. \end{cases} \tag{92}$$

In this paper, different initial conditions are used during simulation. The first kind is so-called normal diffusion process, i.e., I_1. This initial condition is given by

$$c(x_3,0) = \begin{cases} c_{s1}, & x_3 = 0, \\ c_{\mathrm{ref1}} & 0 < x_3 \le L_1, \\ c_{s2} & x_3 = L_1, \\ c_{\mathrm{ref2}}, & L_1 < x_3 \le L_2. \end{cases} \tag{93}$$

The initial condition I_1 can be commonly used to predict the formation and growth of diffusion parts with a bilayer structure. Another kind of condition is the diffusion process with a previous diffusion treatment, i.e., I_2. The depth-dependent initial concentration is approximated to error function, i.e.,

$$c(x_3, 0) = \begin{cases} (c_{s1} - c_{\text{ref1}})[1 - \text{erf}(A_1 x_3)], & 0 \le x_3 \le L_1, \\ (c_{s2} - c_{\text{ref2}})[1 - \text{erf}(A_2 x_3)], & L_1 < x_3 \le L_2. \end{cases} \tag{94}$$

3. Numerical Calculation

Figure 3 schematically shows the algorithm flowchart of the finite difference method (FDM) used in the calculation. The average concentration is the main variable. Within each time step, the volume fraction as well as effective diffusivity and mechanical properties are estimated from average concentration. Based on these values, the diffusion flux, concentration increment and interface movement are predicted.

As shown in Fig. 4, the space domain is divided into $(n-1)$ equally-spaced intervals of space step, Δx. The interface lies between the rth and $(r+1)$th nodes, and the fraction, p, is determined as

$$p = \frac{x_3 - (r-1)\Delta x}{\Delta x}. \tag{95}$$

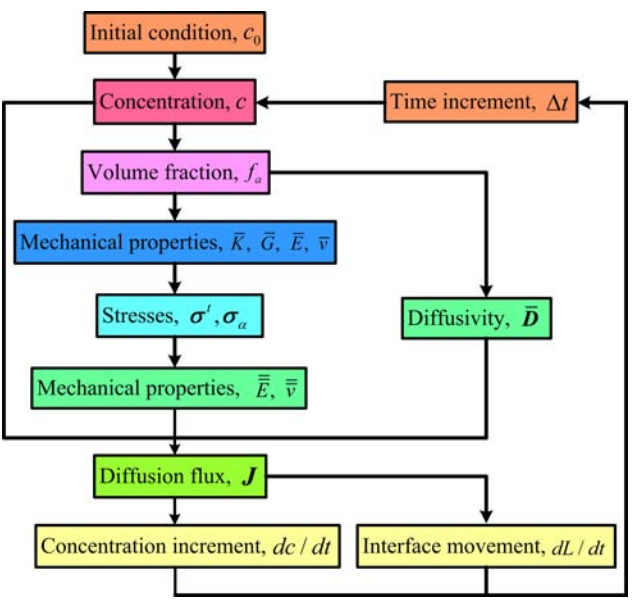

Fig. 3. The flowchart of computational algorithm.

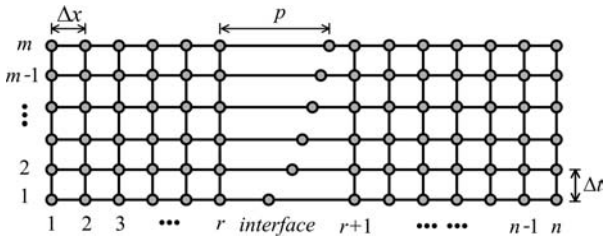

Fig. 4. Space and time grids used in finite difference calculations.

The central difference method is used, i.e.,

$$\left.\frac{df}{dx_3}\right|_{x_3=s\Delta x} = \frac{f_{s+1} - f_{s-1}}{2\Delta x}, \tag{96}$$

$$\left.\frac{d^2 f}{dx_3^2}\right|_{x_3=s\Delta x} = \frac{f_{s+1} + f_{s-1} - 2f_s}{(\Delta x)^2}, \tag{97}$$

where s denotes arbitrary node. As noted by Crank [1957], the singularity arises as p approaches to either limits, i.e., 0 or 1. In order to avoid this problem, Crank [1957] and Zhou and North [1993] used Lagrange's interpolation for approximation, i.e.,

$$f(x_3) = \sum_{k=0}^{n} \left[\left(\prod_{\substack{j=0 \\ j \neq k}}^{n} \frac{x_3 - a_j}{a_k - a_j} \right) f(a_k) \right], \tag{98}$$

where a_j denotes interpolating node, n is the amount of interpolating nodes. If n is as large as 2, the first-order and second-order derivatives can be expressed as

$$\frac{d^2 f(x_3)}{dx_3^2} = 2\left[\frac{f(a_0)}{(a_0 - a_1)(a_0 - a_2)} + \frac{f(a_1)}{(a_1 - a_0)(a_1 - a_2)} + \frac{f(a_2)}{(a_2 - a_0)(a_2 - a_1)} \right], \tag{99}$$

$$\begin{aligned} \frac{df(x_3)}{dx_3} = {} & \frac{(x_3 - a_1) + (x_3 - a_2)}{(a_0 - a_1)(a_0 - a_2)} f(a_0) \\ & + \frac{(x_3 - a_2) + (x_3 - a_0)}{(a_1 - a_0)(a_1 - a_2)} f(a_1) + \frac{(x_3 - a_0) + (x - a_1)}{(a_2 - a_0)(a_2 - a_1)} f(a_2). \end{aligned} \tag{100}$$

At the left-hand side of the interface, we let

$$a_0 = r - 2, \quad a_1 = r - 1, \quad a_2 = r + p. \tag{101}$$

Then the following equations can be obtained as:

$$\left.\frac{d^2 f(x_3)}{dx_3^2}\right|_{x_3=(r-1)\Delta x} = \frac{2}{p+2} f_{r-2} - \frac{2}{p+1} f_{r-1} + \frac{2}{(p+1)(p+2)} f_{r+p}, \tag{102}$$

$$\left.\frac{df(x_3)}{dx_3}\right|_{x_3=(r-1)\Delta x} = -\frac{p+1}{p+2} f_{r-2} + \frac{p}{p+1} f_{r-1} + \frac{1}{(p+1)(p+2)} f_{r+p}, \tag{103}$$

$$\left.\frac{df(x_3)}{dx_3}\right|_{x_3=(r+p)\Delta x} = \frac{p+1}{p+2} f_{r-2} - \frac{p+2}{p+1} f_{r-1} + \frac{3+2p}{(p+1)(p+2)} f_{r+p}, \tag{104}$$

$$f(x_3)|_{x_3=r\Delta x} = -\frac{p}{p+2} f_{r-2} + \frac{2p}{p+1} f_{r-1} + \frac{2}{(p+1)(p+2)} f_{r+p}. \tag{105}$$

At the right-hand side of the interface, we take

$$a_0 = r+p, \quad a_1 = r+2, \quad a_2 = r+3. \tag{106}$$

Then the following equations can be obtained as:

$$\left.\frac{d^2 f(x_3)}{dx_3^2}\right|_{x_3=(r+2)\Delta x} = \frac{2}{(2-p)(3-p)} f_{r+p} - \frac{2}{2-p} f_{r+2} + \frac{2}{3-p} f_{r+3}, \tag{107}$$

$$\left.\frac{df(x)}{dx}\right|_{x=(r+2)\Delta x} = -\frac{1}{(2-p)(3-p)} f_{r+p} - \frac{1-p}{2-p} f_{r+2} + \frac{2-p}{3-p} f_{r+3}, \tag{108}$$

$$\left.\frac{df(x)}{dx}\right|_{x=(r+p)\Delta x} = \frac{2p-5}{(2-p)(3-p)} f_{r+p} + \frac{3-p}{2-p} f_{r+2} - \frac{2-p}{3-p} f_{r+3}, \tag{109}$$

$$f(x)|_{x=(r+1)\Delta x} = \frac{2}{(2-p)(3-p)} f_{r+p} + \frac{2(1-p)}{2-p} f_{r+2} - \frac{1-p}{3-p} f_{r+3}. \tag{110}$$

Figure 5 schematically shows the movement of interface. Regions I and II indicate the concentration increment at the nodes far away from interface. The shaded area including regions III–V, denotes the concentration accumulation involved with interface movement. Its value, ΔS, is expressed as

$$\Delta S = (J_{i1} - J_{i2})\Delta t, \tag{111}$$

where J_{i1} and J_{i2} are the flux at the left-hand and right-hand side of interface. Then the moving rate of interface can be easily evaluated as

$$\frac{dL_1}{dt} = \frac{\Delta S}{\Delta t} = \frac{2(J_{i1} - J_{i2})}{c_{\text{ref1}} - c_{s2} + c_r - c_{r+1}}, \tag{112}$$

where c_{i1} and c_{i2} are the concentration at the left-hand and right-hand side of interface. When the area of III is much larger than, IV and V, Eq. (112) can be simplified to

$$\frac{dh_{ox}}{dt} = \frac{J_{i1} - J_{i2}}{c_{\text{ref1}} - c_{s2}}, \tag{113}$$

which is widely used in previous modeling work. Compared with Eq. (113), Eq. (112) has effectively avoided the appearance of singularity when the difference between

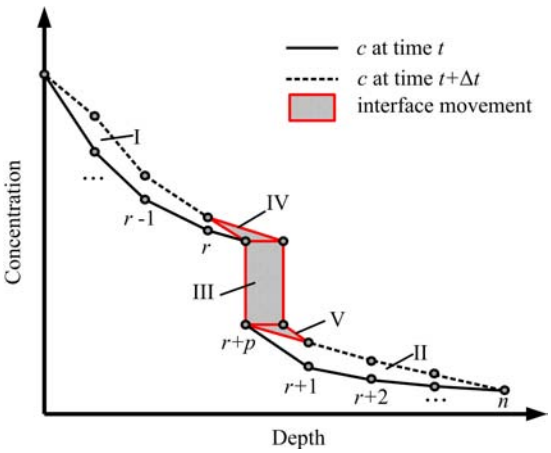

Fig. 5. The movement of interface and the concentration increment near it.

c_{ref1} and c_{s2} approaches to zero. If the interface passes the ith node, the composition change due to phase transformation can be evaluated by Lagrange's interpolation. If the interface moves to the substrate side,

$$c_i = -\frac{(i-r+1)(i-\tilde{r}-\tilde{p})}{r-2-\tilde{r}-\tilde{p}}c_{r-2} + \frac{(i-r+2)(i-\tilde{r}-\tilde{p})}{r-1-\tilde{r}-\tilde{p}}c_{r-1} + \frac{(i-r+2)(i-r+1)}{(\tilde{r}+\tilde{p}-r+2)(\tilde{r}+\tilde{p}-r+1)}c_{r+p}, \tag{114}$$

where $\tilde{r}$ and $\tilde{p}$ are the updated r and p after the time step. If the interface moves to the oxide side, we have

$$c_i = -\frac{(i-r-2)(i-r-3)}{(\tilde{r}+\tilde{p}-r-2)(\tilde{r}+\tilde{p}-r-3)}c_{r+p} - \frac{(i-\tilde{r}-\tilde{p})(i-r-3)}{r+2-\tilde{r}-\tilde{p}}c_{r+2} + \frac{(i-\tilde{r}-\tilde{p})(i-r-2)}{r+3-\tilde{r}-\tilde{p}}c_{r+3}. \tag{115}$$

4. Results and Discussions

The property parameters of two different composites, C1 and C2, are presented in Table 1. For simplicity, each composite consists of matrix and unique inclusion phase.

4.1. *Effective diffusivity and mechanical properties*

The variation of effective diffusivity along with inclusion volume fraction is shown in Fig. 6. The composite C1 is chosen for calculation. When the diffusivity of inclusion is larger than that of matrix, the effective diffusivity increases with increasing the inclusion volume fraction. At the left and right end of the horizontal axis,

Table 1. Property parameters of composites C1 and C2 used in calculation.

	Composite 1 (C1)	Composite 2 (C2)
K_0 (GPa)	100	70
G_0 (GPa)	45	40
K_α (GPa)	150	80
G_α (GPa)	70	48
D_0 ($m^{-1}s^{-1}$)	30e − 15	10e − 16
D_α ($m^{-1}s^{-1}$)	10e − 15	30e − 16
c_s (.1)	0.8	0.10
c_{ref} (.1)	0.2	0.01
H (.1)	0.0012	0.003
η (m^3mol^{-1})	1e − 5	1e − 5
T (K)	273.15	273.15
Δt (s)	1	1
Δx (μm)	1e − 6	1e − 6

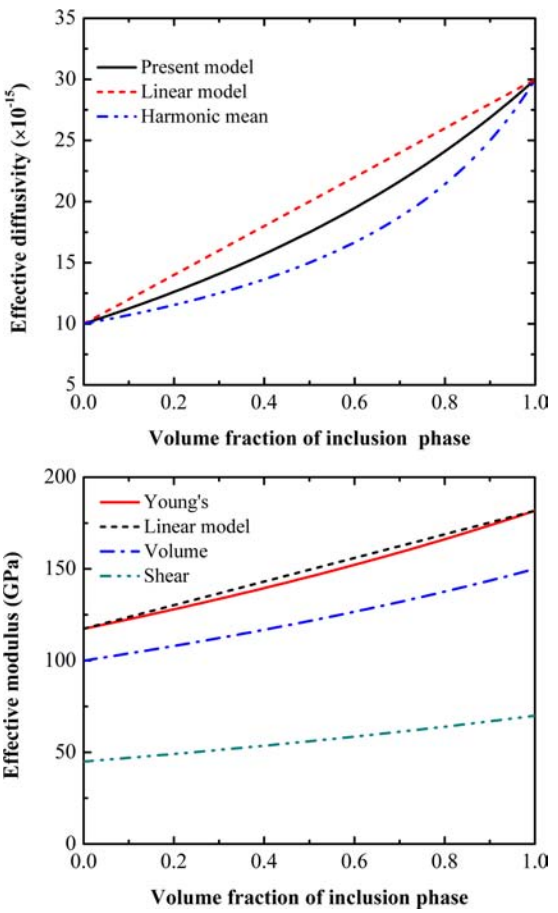

Fig. 6. Variation of effective diffusivity and elastic properties along with inclusion volume fraction.

the effective value equals to the diffusivity of matrix and inclusion. As comparison, the arithmetical and harmonic means are also presented in Fig. 6, which were employed in previous prediction of effective diffusivity [Yang, 2005]. The homogenization result lies between the arithmetical and harmonic means. The variation of effective modulus along with volume fraction of inclusion phase are also shown in Fig. 6. Similar to the homogenization on diffusivity, the composite C1 is chosen for the calculation. The effective Young's modulus, volume and shear modulus change monotonically with the volume fraction of the inclusion. When the volume fraction reaches 0 or 1, the effective modulus become equal to the values of pure matrix or inclusion phase. If the matrix is the dominated phase, linear relationship between Young's modulus and volume fraction was widely used to evaluate the Young's modulus of composites. As a reference, the arithmetical mean of Young's modulus is also presented in Fig. 6. The homogenization result is generally smaller compared with the arithmetical mean, especially in the central region of the horizontal axis.

4.2. *Normal diffusion process*

Figure 7 shows the concentration variation along with the depth with respect to different oxidation time. The maximum time for diffusion is set to be 100,000 s. The outer and inner parts are respectively composed of C1 and C2. Initial condition I_1 is selected before calculation, where initial L_1 and L_2 are given by 3 and 100. As seen in Fig. 7, concentration decreases with the distance from the surface to form a specific gradient structure within each part. The concentration at a specific location point generally increases with time. At the left boundary and interface, the concentration remains constant due to the boundary condition. At the right boundary, the partial derivative of concentration with respect to depth is identically vanishing. The simulation results also reveal the growth process of the outer part through the phase transformation from C2 into C1. The diffusing element are consumed through two ways, i.e., accumulating at the interface to move the interface forward or diffusing into the inner part to raise the concentration up. At the very initial stage, additional elements would prefer to diffuse within each part, changing the piecewise-step function to a linear function. After that, the interface begins to move rapidly and its movement will be decelerated with the passage of time. The detailed concentration distribution along with depth with respect to different diffusion time is also presented in Fig. 7. Figure 8 shows the stress variation along with the depth with respect to different oxidation time. It is clear that the stress changes from compressive to tensile at the position near the interface.

According to Eshelby's theory, the total stress is the sum of disturbance stress and average stress. The disturbance within the interior of inclusion domain is independent of location. While that in the exterior part decreases with the distance from inclusion domain and difficult to calculate. The relationship among average stress, disturbance stress, and total stress within the inclusion domain is given by Fig. 9.

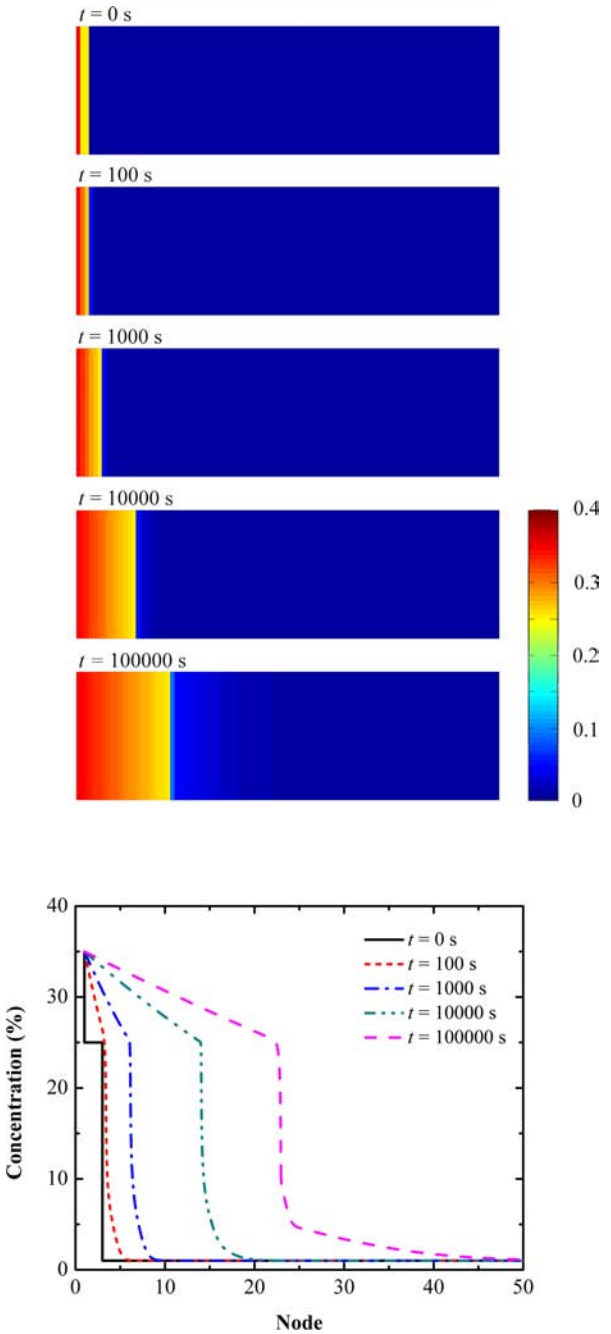

Fig. 7. Concentration variations along with the depth with respect to different oxidation times. The maximum time for diffusion is set to be 100,000 s. The initial condition I_1 is selected before calculation, where initial values of L_1 and L_2 are given as 3 and 100. Color contour is the dimensionless concentration (Color online).

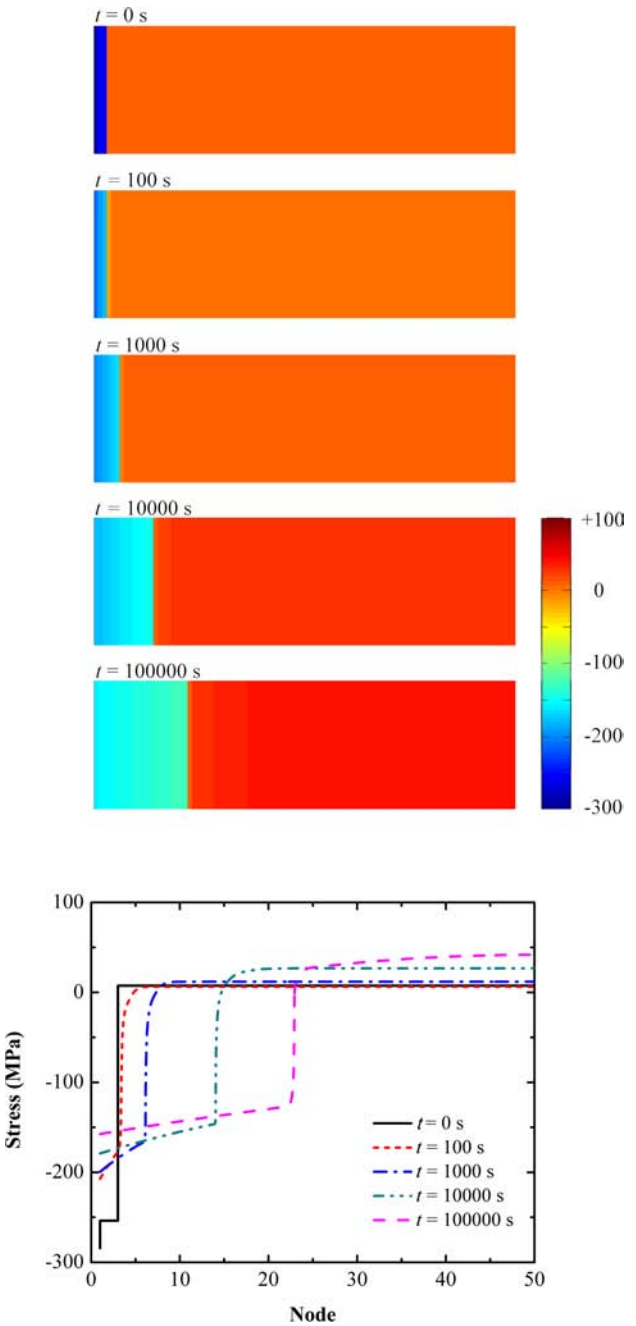

Fig. 8. Stress variation along with the depth with respect to different oxidation time. The maximum time for diffusion is set to be 100,000 s. Initial condition I_1 is selected before calculation, where initial L_1 and L_2 are given by 3 and 100. Color contour is the normal stress contour with unit MPa (Color online).

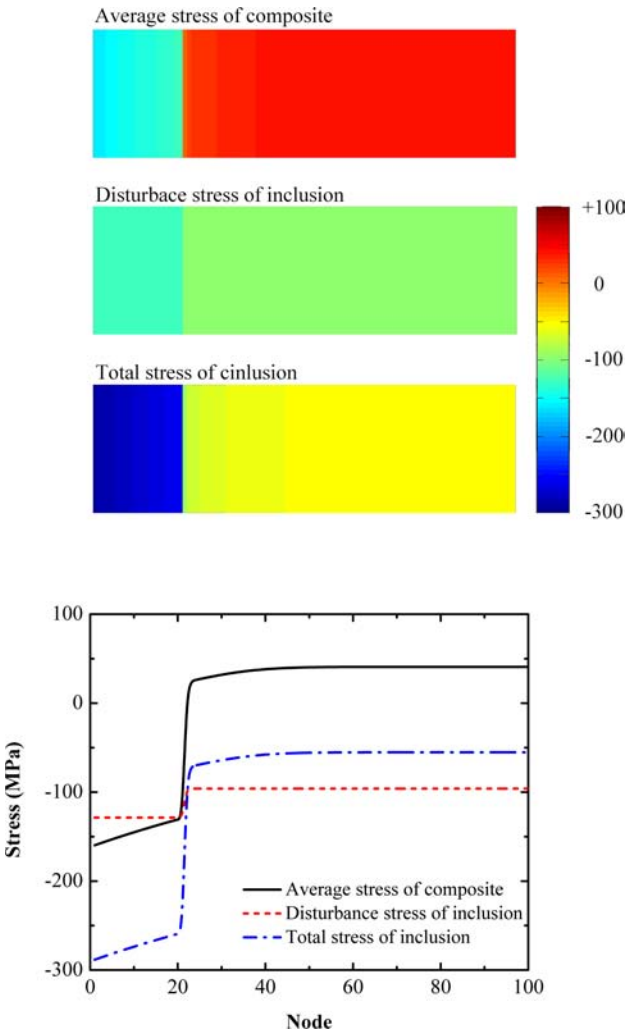

Fig. 9. Variation of average stress, disturbance stress, and total stress along with depth after diffusion for 100,000 s. Initial condition I_1 is selected before calculation, where initial L_1 and L_2 are given by 3 and 100. Color contour is the normal stress with unit MPa (Color online).

Resulted from the lattice expansion, the inclusion phases are generally under compressive stress. Since the concentration within the specific inclusion phase is given, the disturbance stress remains constant within inner and outer parts of the material. The average stress is determined by average concentration. Compressive and tensile stress are respective obtained in the inner and outer parts. The compressive stress decreases with decreasing average concentration. As the sum of the disturbance stress and average stress, the total stress of the inclusion phase is generally compressive.

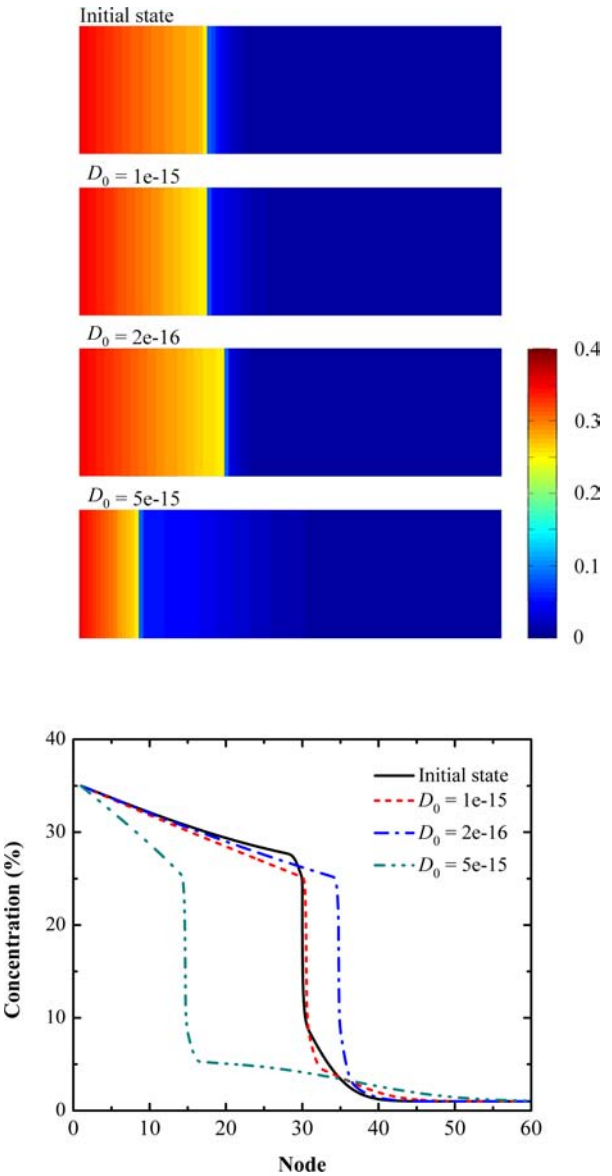

Fig. 10. Concentration variation along with the depth with respect to different oxidation time. The maximum time for diffusion is set to be 100,000 s. Initial condition I_1 is selected during calculation, where initial L_1 and L_2 are given by 30 and 100. Color contour is the dimensionless concentration (Color online).

4.3. *Diffusion process with previous diffusion*

Figure 10 shows the simulation results of diffusion process with previous diffusion treatment. During the performance of simulation, the initial condition I_2 is selected,

where L_1 and L_2 are set to be 30 and 100. Other parameters remain unchanged. The subsequent diffusion and interface movement are shown to be greatly affected by the diffusivity. During the previous diffusion process, the concentration distribution has reached a relatively stationary state, i.e., the flux difference between the two sides of interface is very small. The abrupt change of diffusivity will break the balance and induce the movement of interface. For the case $D_0 = 1\mathrm{e} - 15$, there is no significant change of concentration distribution and interface position over time. For the case $D_0 = 2\mathrm{e} - 16$, the decrease of the diffusivity in C2 will result in the accumulation of diffusing element at the interface and the following phase transformation. For the case $D_0 = 5\mathrm{e} - 15$, the thickness of outer part is increased sharply with increasing the diffusivity in C2 and directly induce the decomposition of C1 as well as the formation of C2.

5. Conclusions

The following conclusions may be drawn from the present study:

(1) A comprehensive model has been developed for coupled mechanical-diffusion problem with moving interface. The diffusion process and stress condition are shown to affect each other. The homogenization on mechanical properties and diffusivity is considered during modeling.
(2) The simulation on the diffusion problem with moving boundary is performed. A modified FDM is employed during simulation.
(3) Two situations are considered in the present model, i.e., normal diffusion process and that with previous diffusion. In the latter case, the outer part could decompose to maintain the further diffusion within the inner part.

Acknowledgments

The author would like to acknowledge gratefully for the financial support through National Natural Science Foundations of China (51371082 and 51322510). The author Xian-Cheng Zhang is also grateful for the support by Shanghai Pujiang Program, Young Scholar of the Yangtze River Scholars Program, and Shanghai Technology Innovation Program of SHEITC (CXY-2015-001).

References

Anand, L. [2012] "A Cahn–Hilliard-type theory for species diffusion coupled with large elastic-plastic deformations," *Journal of the Mechanics and Physics of Solids* **60**(12), 1983–2002.

Bhandakkar, T. K. and Johnson, H. T. [2012] "Diffusion induced stresses in buckling battery electrodes," *Journal of the Mechanics and Physics of Solids* **60**(6), 1103–1121.

Crank, J. [1957] "Two methods for the numerical solution of moving-boundary problems in diffusion and heat flow," *The Quarterly Journal of Mechanics and Applied Mathematics* **10**(2), 220–231.

Dong, H. and Bell, T. [2000] "Enhanced wear resistance of titanium surfaces by a new thermal oxidation treatment," *Wear* **238**(2), 131–137.

Eshelby, J. D. [1957] "The determination of the elastic field of an ellipsoidal inclusion, and related problems," *Proceedings of the Royal Society A* **241**(1226), 376–396.

Güleryüz, H. and Çimenoğlu, H. [2004] "Effect of thermal oxidation on corrosion and corrosion-wear behaviour of a Ti-6Al-4V alloy," *Biomaterials* **25**(16), 3325–3333.

Haftbaradaran, H., Song, J., Curtin, W. A. and Gao, H. [2011] "Continuum and atomistic models of strongly coupled diffusion, stress, and solute concentration," *Journal of Power Sources* **196**(1), 361–370.

Kuhn, R., Michelitsch, T., Levin, V. M. and Vakulenko, A. A. [2002] "The analogue of the Eshelby tensor for a piezoelectric spheroidal inclusion in the hexagonal electroelastic medium," *Journal of Applied Mathematics and Physics* **53**(4), 584–602.

Larchè, F. C. [1978] "A nonlinear theory of thermochemical equilibrium of solids under stress," *Acta Metallurgica* **26**(1), 53–60.

Lazaridis, A. [1970] "A numerical solution of the multidimensional solidification (or melting) problem," *International Journal of Heat and Mass Transfer* **13**(9), 1459–1477.

Li, J. Y. and Dunn, M. L. [1998] "Anisotropic coupled-field inclusion and inhomogeneity problems," *Philosophical Magazine A* **77**(5), 1341–1350.

Li, S. and Wang, G. [2008] *Introduction to Micromechanics and Nanomechanics* (World Scientific Publishing, USA).

Maharjan, S., Zhang, X. C. and Wang, Z. D. [2012] "Analytical modeling of stress and strain of symmetrically oxidized metal," *Journal of Applied Physics* **112**(3), 033514.

Mori, T. and Tanaka, K. [1973] "Average stress in matrix and average elastic energy of materials with misfitting inclusion," *Acta Metallurgica* **21**(5), 571–574.

Mura, T. [1987] *Micromechanics of Defects in Solids* (Kluwer Academic Publishers Group, Dordrecht, The Netherlands).

Rosa, C. J. [1970] "Oxygen diffusion in alpha and beta titanium in the temperature range of 932° C and 1142° C," *Metallurgical Transactions* **1**(9), 2517–2522.

Schuh, C. [2000] "Modeling gas diffusion into metals with a moving-boundary phase transformation," *Metallurgical and Materials Transaction A* **31**(10), 2411–2421.

Tanaka, K. and Mori, T. [1972] "Note on volume integrals of the elastic filed around an ellipsoidal inclusion," *Journal of Elasticity* **2**(3), 199–200.

Villani, A., Busso, E. P., Ammar, K., Forest, S. and Geers, M. G. D. [2014] "A fully coupled diffusional-mechanical formulation: Numerical implementation, analytical validation, and effects of plasticity on equilibrium," *Archive of Applied Mechanics* **84**(9), 1647–1664.

Weng, G. J. [1990] "The theoretical connection between Mori–Tanaka's theory and the Hashin–Shtrikman–Walpole bounds," *International Journal of Engineering Science* **28**(11), 1111–1120.

Wu, C. H. [2001] "The role of Eshelby stress in composition-generated and stress-assisted diffusion," *Journal of the Mechanics and Physics of Solids* **49**(8), 1771–1794.

Yang, F. [2005] "Interaction between diffusion and chemical stresses," *Material Science and Engineering A* **409**(1–2), 153–159.

Zhang, Y., Ma, G. R., Zhang, X. C., Li, S. and Tu, S. T. [2016] "Thermal oxidation of Ti-6Al-4V alloy under external bending strain: Experiment and modelling," Submitted to *Corrosion Science*.

Zhang, Y., Zhang, X. C. and Tu, S. T. [2015] "Coupled mechanical-oxidation modeling during silicon thermal oxidation process," *AIP Advances* **5**(9), 097105.

Zhang, Y., Zhang, X. C., Tu, S. T. and Xuan, F. Z. [2014] "Analytical modeling on stress assisted oxidation and its effect on creep response of metals," *Oxidation of Metals* **82**(3), 311–330.

Zhou, Y. and North, T. H. [1993] "Kinetics modelling of diffusion-controlled, two phase moving interface problems," *Modelling and Simulation in Materials Science and Engineering* **1**(4), 505–516.

Zumpicchiat, G., Pascal, S., Tupin, M. and Berdin-Méric, C. [2015] "Finite element modelling of the oxidation kinetics of Zircaloy-4 with a controlled metal-oxide interface and the influence of growth stress," *Corrosion Science* **100**, 209–221.